CHAPTER 305

An Energetics Approach for Suspended Sand Transport on Macrotidal Ridge and Runnel Beaches

George Voulgaris[1], Travis Mason[2] and Michael B. Collins[2]

Abstract

High frequency observations of hydrodynamics and suspended sediment concentration were acquired from the intertidal zone of a macrotidal ridge and runnel beach. The hydrodynamic data from the electromagnetic current meters were used to calculate sediment transport rates according to Bailard's (1981) energetics model. Additionally, suspended sediment fluxes were calculated for the period of data collection. The contribution of long waves, short waves and mean currents to suspended sediment transport was examined. Application of the energetics model suggested that suspended sediment is the dominant mode of transport. Further, it showed that the waves define net sediment transport rate and direction. However, the measurements revealed that the transport due to mean currents was dominant. The discrepancy between the model and measurements was attributed to vortex ripples which were developed in the intertidal zone. Bailard's model failed to predict the oscillatory mode of transport but it was found to predict accurately the mean mode of suspended sediment transport assuming an efficiency factor value of 0.021 is used in the calculations.

Introduction

Sand resuspension under the action of waves and currents is the primary process controlling seabed erodibility. Successful parameterization of this mechanism is the key element for the development of accurate and predictive morphological models. Presently, Bailard's (1981) sediment transport formula is considered one of the best theoretical models for time-dependent, cross-shore sediment transport (Schoonees and Theron, 1995) and is widely used for the prediction of changes in the coastal zone (*e.g.* Scott *et al.*, 1991). The model is based on the importance of various moments of the fluid velocity in determining transport rates. Previous studies examined the various velocity moments

[1]Woods Hole Oceanographic Institution, Woods Hole, MA 02543, U.S.A.

[2]Department of Oceanography, University of Southampton, Southampton Oceanography Centre, European Way, Southampton, SO14 3ZH, U.K.

under either wave (*i.e.*, Guza and Thornton, 1985; Russell *et al.*, 1995) or steady current dominating conditions (*i.e.*, Thornton *et al.*, 1996). Ridge and runnel beaches, however, are found throughout areas with moderate wave conditions (short-fetched seas) and high tidal ranges (King and Williams, 1949; Orford and Wright, 1978). The combination of high tidal currents and moderate wave activity invalidates the assumptions of the previous investigators regarding the dominant forces (*i.e.* waves or steady currents).

In this contribution, high frequency measurements of instantaneous currents and suspended sediment concentration were obtained on a macrotidal ridge and runnel beach. The data collected are used to: (i) examine determine the relative contributions of long waves, short waves and mean currents to suspended sediment transport; (ii) evaluate the energetics sediment transport model (Bailard, 1981) and velocity moments for macrotidal conditions; and (iii) calibrate the energetics model for suspended sand transport.

Energetics Model

Bagnold's (1966) energetics-based total load sediment transport model for streams has been used as a basis for the development of a model of time-varying transport over a plane sloping bed. The idealised equation for the total (i.e bedload and suspended load, $\langle I_t \rangle$) time-averaged immersed weight sediment transport is given by Bailard (1981):

$$\langle \vec{I}_t \rangle = \rho\, C_f \frac{\epsilon_b}{\tan\phi} \left[\langle |\vec{U}_t|^2 \vec{U}_t \rangle + \frac{\tan\beta}{\tan\phi} \langle |\vec{U}_t|^3 \rangle \vec{i} \right] + \rho\, C_f \frac{\epsilon_s}{W} \left[\langle |\vec{U}_t|^3 \vec{U}_t \rangle + \frac{\epsilon_s}{W} \tan\beta \langle |\vec{U}_t|^5 \rangle \vec{i} \right] \quad (1)$$

where W is the sediment fall velocity; ϵ_b and ϵ_s are the bed load and suspended load efficiency factors, respectively; β is the local bed slope; ϕ is the angle of internal friction of the sediment; i is the unit vector in the down-slope, offshore (-x) direction; and U_t the total instantaneous velocity.

The above general model has been analysed into the cross-shore ($\langle I_x \rangle$) and longshore ($\langle I_y \rangle$) components for application with random waves (Guza and Thornton, 1985):

$$\langle I_x \rangle = \rho C_f U_m^3 \{ \frac{\epsilon_B}{\tan\phi} \cdot [\psi_1 \cos\alpha_1 + \delta_u^3 + \delta_u (\frac{1}{2} + \cos^2\alpha_2 + \delta_u^2) + \delta_u \sin\alpha_3 \cos\alpha_3 + \frac{\tan\beta}{\tan\phi} u3^*] + \frac{U_m}{W} \epsilon_s [\psi_2 \cos\alpha_5 + \delta_u \cdot u3^*] + \frac{U_m^2}{W^2} \epsilon_s^2 \tan\beta \cdot u5^* \quad (2)$$

$$\langle I_y \rangle = \rho \cdot C_f U_m^3 \cdot \{ \frac{\epsilon_B}{\tan\phi} \cdot [\psi_1 \sin\alpha_1 + \delta_v^3 + \delta_v (\frac{1}{2} + \sin^2\alpha_2 + \delta_u^2) + \delta_u \sin\alpha_3 \cos\alpha_3] + \frac{U_m}{W} \epsilon_s [\psi_2 \sin\alpha_5 + \delta_v \cdot u3^*] \quad (3)$$

where U_m is the oscillatory velocity (rms) amplitude. δ_u and δ_v are the steady current strength for the cross-shore and longshore directions defined as $\bar{u}/U_m$ and $\bar{v}/U_m$, respectively. The most important normalised velocity moments are:

$$\psi_1 = \frac{<|U_t|^2(u_{osc}, v_{osc})>}{U_m^3} \quad (4)$$

$$\psi_2 = \frac{<|\vec{U}_t|^3(u_{osc}, v_{osc})>}{U_m^4} \quad (5)$$

where the symbols <> denote a time-averaged quantity. The velocity components are decomposed into an oscillatory (u_{osc}, v_{osc}) and a mean ($\bar{u}$, $\bar{v}$) part, so that:

$$|\vec{U}_t| = \sqrt{u_{osc}^2 + v_{osc}^2 + \bar{u}^2 + \bar{v}^2 + 2(u_{osc}\bar{u} + v_{osc}\bar{v})} \quad (6)$$

The definitions of the remaining parameters can be found in Guza and Thornton (1985, see page 251, eqns 35 and 36). Briefly, αn (n=1 to 5) are the angles associated with the directional characteristics of the various flow moments, while $u3^*$ and $u5^*$ are the odd moments of the total instantaneous flow, integrated over the whole wave period. Application of the above model requires information on the moments of the instantaneous velocity field.

In order to obtain a quantitative prediction of immersed weight sediment transport rate, values for the drag coefficient (C_f) and the efficiency factors are required. Bowen (1980) proposed a value of 0.005 for the drag coefficient. Here, the drag coefficient is determined by the flow conditions as function of the ratio z_o/h (Soulsby *et al.*, 1993). The efficiency factors used in this model are known to depend on factors such as flow conditions (laminar or turbulent, steady or unsteady, etc), and the grain size characteristics of the sediments. A list of various suggested values is presented in Table 1.

Author	Bedload	Suspended load
Bagnold (1966), steady flow	0.13	0.010
Bailard (1981,1982) longshore	0.21	0.025
Bailard (1981,1982), cross-shore	0.10	0.020
Bowen (1981), cross-shore	0.15 tanϕ	0.010

Table 1. Efficiency parameter values proposed by various investigators.

Guza and Thornton (1985) applied field data to Bailard's cross-shore sediment transport model to determine the dominant terms in the bedload and suspended load modes. They concluded that suspended load dominates sediment transport processes and

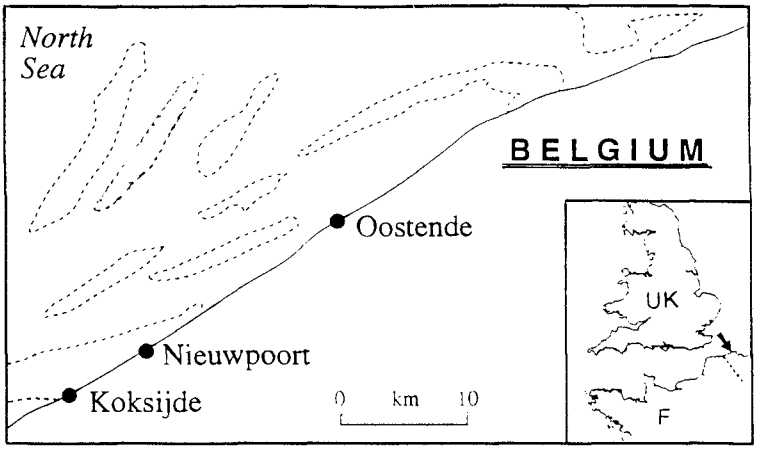

Figure 1. Location of experimental site.

that the normalised velocity moments ψ_2 and $\delta_u u3^*$ are the most important terms, representing the contribution of the oscillatory and mean flow to suspended sediment transport, respectively.

Bowen (1980), Roelvink and Stive (1989), and Russell et al (1996) have extended Guza and Thornton's (1985) work by examining the relative importance of the long, short period oscillations and mean flow to cross-shore suspended sediment transport. Their analysis was based on the assumption that the longshore currents are much smaller than the orbital velocities ($\bar{v}<<U_m$). On the other hand, Thornton et al. (1996) presented an expansion of equation (1) which is based on the assumption that mean currents dominate the flow.

Macro-tidal ridge and runnel beaches are found though, throughout areas with moderate wave conditions (short fetched seas); this, combined with the high tidal currents invalidates the assumptions used by the above investigators. In the present analysis the velocity terms of eqns (2) and (3) are examined, assuming that both waves and currents are of equal importance. In addition, almost all of the above studies concentrated on the cross-shore direction only. Due to the importance of the longshore tidally-induced currents found on ridge and runnel beaches it is considered appropriate that both horizontal components (cross-shore and longshore) should be included in the velocity moments analysis.

Experimental Site - Data Collection

The field measurements were obtained at Nieuwpoort-aan-Zee, situated some 13km southwest of Oostende (Fig. 1), from 20th February to 4th March 1994 (Julian days 51-63). The experimental site was outside the influence of any man-made obstructions, such as groynes which are typical elsewhere. The sediment is well sorted, fine/medium sand (mean grain size 0.183mm); at the time of the observations the average beach slope ($\tan\beta$) was 0.012 with an intertidal zone of between 250 and 500m wide. The

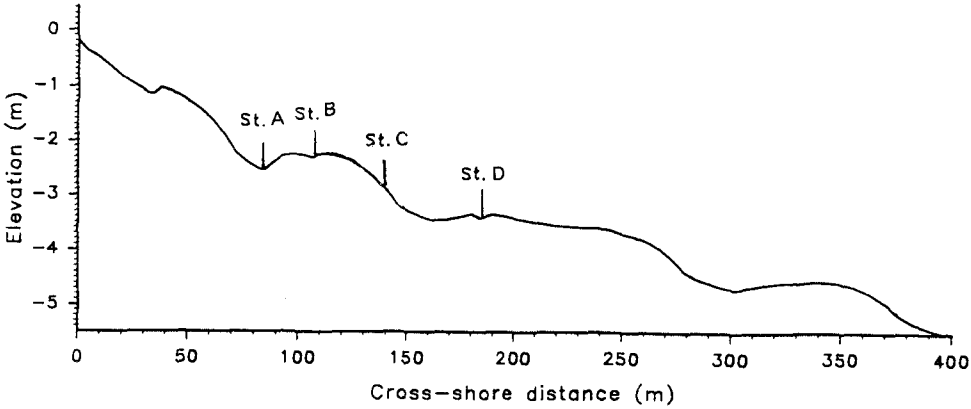

Figure 2. Cross-sectional profile of the intertidal zone and locations of instrument stations (A, B, C and D).

experimental site exhibited typical ridge and runnel beach characteristics (Fig. 2) with up to five well defined ridges exposed at low tide.

Tides in this area are semi-diurnal with a large neap to spring variation of 2.7 to 6.5m during the deployment period. Offshore currents are characterised by elongate and asymmetrical tidal current ellipses, with a northeasterly directed residual flood displacement controlling the sub-tidal sediment transport pathways (De Moor, 1991).

The wave climate of the area is typical of short-fetched seas with wave periods 3 to 6s. However, typical wave periods recorded during the deployment period were between 4 and 12 seconds with offshore wave heights of the order of 0.5 to 1m. Dominant offshore wave direction, extracted from wave hindcasting modelling (U.K. Meteorological Office), is primarily from the west-southwest (23% of the time) and secondarily from the north-northeast (10% of the time).

Four instrumented stations were deployed in the intertidal zone (Fig. 2). The instruments deployed consisted of electromagnetic current meters (Stations A, B, C and D), pressure transducers (Stations B, C and D) and optical backscatter sensors (OBS) for measuring instantaneous suspended sediment concentration (SSC, Stations C and D). The OBS data obtained from station C were of too poor quality to be used for analysis. Therefore, the results presented here are based on the data collected at Station D which was located in the upper mid-tidal zone and on the top of a ridge with a relatively flat crest (Figure 2).

Four 2-axis electromagnetic current meters, 3 OBS sensors and a pressure transducer were deployed at station D. All instruments were cantilevered from a stainless steel pipe, set vertically into the beach sand during low water. Three of the electromagnetic current meters were arranged to measure instantaneous horizontal currents at three levels above the sea bed (21.5, 48 and 108.5cm, respectively). The fourth sensor was orientated to measure vertical currents at 70cm above the sea bed. The OBS sensors were installed at elevations 9, 19 and 34.5cm above the sea bed, respectively. Data were collected when

the instruments were fully submerged and for consecutive time intervals of approximately 17min, spanning flood, high water and ebb tide. The sampling frequency within each burst was 8 Hz.

Sediment from the deployment area was used for the calibration of the OBS sensors. A temporally variable background level of "turbidity" was observed during the data collection period. This was due to fine material in suspension, referred t hereafter as "washload", coming from Nieuwpoort Harbour. To maintain uniformity in data analysis, the offset due to this washload was determined as the 10th percentile of the sample values as suggested by Aagaard and Greenwood (1995). This was the magnitude of concentration which corresponded approximately to a significant break in the cumulative frequency of signal values and best represents the separation between the background signal and sediment resuspension events. As Aagaard and Greenwood (*op. cit.*) noted such an approach may introduce some error in computing absolute magnitudes of sediment transport rates. Laboratory experiments showed that this error is less than 10%.

Hydrodynamic and suspended sediment concentration measurements were obtained during 3 tidal cycles on 3rd and 4th March, 1994 (Julian days 62 and 63, respectively). In particular, 6 data sets (runs) were collected during the flood of the morning flood tide of Julian day 62; 9 runs during the evening of Julian day 62; and finally 12 runs were collected during the morning of Julian day 63.

Time-series of cross-shore and longshore velocity (u,v) and sediment concentration (c) were plotted to check data quality. Statistical descriptions of velocity and sediment concentration were computed (i.e mean and standard deviations). Wave characteristics were computed using the moments of the spectra of the pressure transducer signal after correcting for depth attenuation (Voulgaris, 1992). Significant orbital velocities were estimated from the standard deviation of each time-series ($U_m=(2(u_\sigma^2+v_\sigma^2))^{1/2}$).

The total fluxes have been analysed into mean and oscillatory modes with the latter being decomposed further into fluxes due to incident short (gravity, subscript $_S$) waves and long period (infragravity, subscript $_L$) flow.

$$\overline{u \cdot c} = \bar{u} \cdot \bar{c} + \overline{u_{osc} \cdot c_{osc}} = \bar{u} \cdot \bar{c} + \overline{u_S \cdot c_S} + \overline{u_L \cdot c_L} \qquad (7)$$

The mean component was calculated (by averaging the entire 17 minute record), and then subtracted from the record, to obtain the oscillatory component. The infragravity (long) component of the signal (u_L, v_L and c_L) was calculated by applying a low-pass filter (cut-off frequency 0.06Hz) to the oscillatory component. The infragravity component was subtracted from the total oscillatory component, thus giving the gravity contribution.

Local fluxes were calculated for each data run according to eqn. (7), for both the cross-shore and longshore directions and for the three elevations above the sea bed where SSC measurements were obtained. Measurements from the current meter installed at 21.5cm above the sea bed were used for the local flux calculations. Oscillatory currents were assumed to be constant through the water column whilst a logarithmic distribution was assumed for estimating the fluxes due to mean currents.

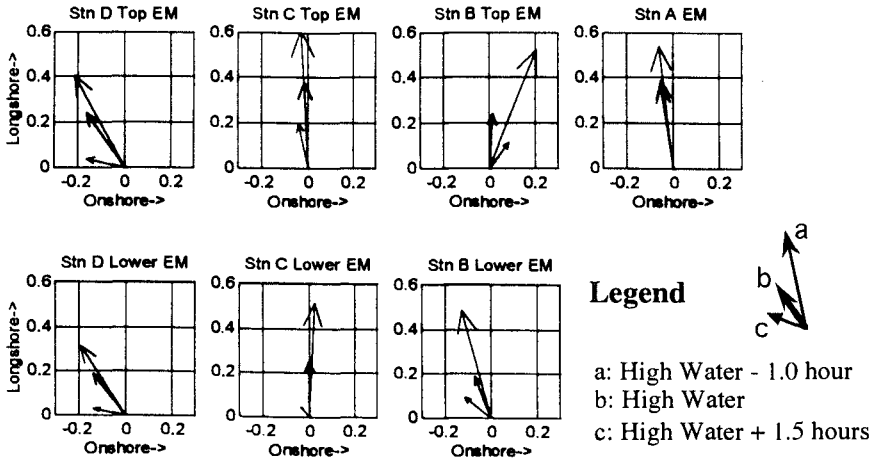

Figure 3. Vector diagrams of mean flow in the intertidal zone (for locations see Fig. 2) at 1 m (top row) and 0.2m (bottom row) above the sea bed (units in m/s).

Results

Overview of Hydrodynamics

In this section an overview of the hydrodynamic conditions in the intertidal zone is presented. This is based on observations from the whole of the experimental period. Typical mean flow patterns in the intertidal zone were found to be tidally-induced. Figure 3 shows the magnitude and direction of the mean current, for a typical tide, before (-1 hour) during and after (+1.5 hours) high water. It is evident that the dominant flow direction is consistently alongshore in the positive (northeast) direction. Maximum longshore flow occurs during the flood stage of the tide and the magnitude of the longshore current reduces as the tide progresses. Preliminary analysis of the hydrodynamic data collected indicates the this behaviour is due to bed friction which causes the longshore currents to lead the tidal elevation inshore. The mean cross-shore flow is generally offshore for all stations. An exception to this is Station B where the currents at 1 m above the bed are generally directed onshore. This station is located at the top of a ridge (see Fig. 2) where the waves exhibit their maximum asymmetry, thus this onshore flow is attributed to onshore mass transport which is balanced by an offshore flow near the seabed.

The wave climate in the intertidal zone exhibits a dependence on tidal stage (ebb, flood, see Figure 4). Local wave height is larger during the flood than during the ebb stage of the tide. This is more enhanced at the offshore stations C and D). This wave height dependence on tidal stage is the result of the interaction of the waves with the tidally-induced longshore currents. During flood, the currents are strongest and are directed toward the northeast. This results in the currents opposing the surface waves which, during the time of observation, were propagating at an angle towards the southwest. This

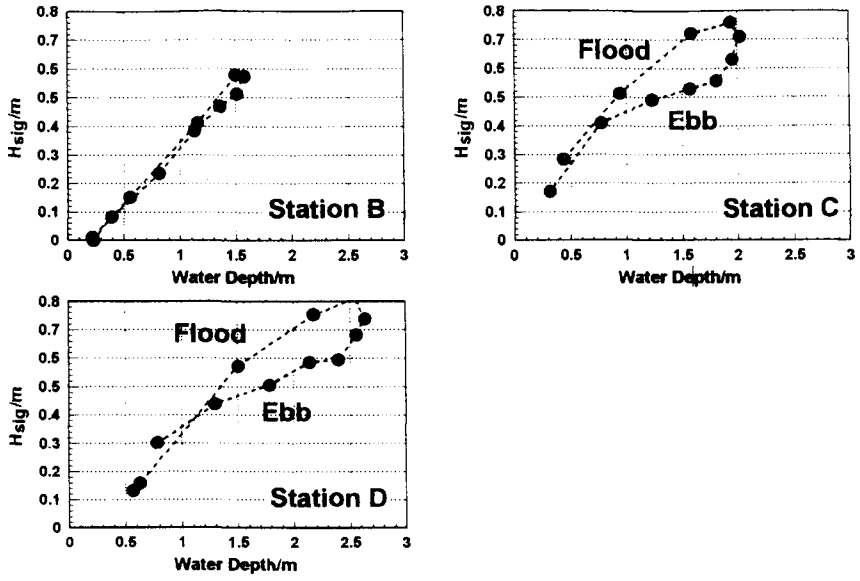

Figure 4. Tidal modulation of the local wave height (H_{sig}) for stations B, C and D (for location see Fig. 2).

opposition of waves and currents resulted in an increased wave steepness. During the ebb stage of the tide, the current strength is significantly reduced (see Figure 3), so that the interaction is much lesser, leading into less steep waves.

Velocity Moments

The relevant flow moments to sediment transport are examined in order to identify the most important terms for macrotidal beaches. Following Guza and Thornton's (1985) approach, the field flow data collected at station D from the lowest current meter are used to estimate the terms of eqns. (2) and (3).

The values of the individual terms such as ψ_1, ψ_2, $u3^*$, $u5^*$, δ_u, δ_v and the angles α_1,α_2, α_3, and α_5 have been evaluated for each run during the data collection period and the results are shown in Figure 5. The nonlinear scalar moments ψ_1 and ψ_2 are linked in the transport eqns (2) and (3) to the angles α_1 and α_5. The moments ψ_1 and ψ_2, (Fig. 5a) are associated with the wave asymmetry and this is why their variation through the tidal cycles corresponds to the variation in the wave orbital velocity field, as discussed in the previous section (see Fig. 4). However, in the case of a dominant cross-shore oscillatory component, the angles α_1 and α_5 in the case of a dominant cross-shore oscillatory components are expected to by around zero or 180degs (Guza and Thornton, 1985). In the present data set though α_1 varies between -10 and 10 degs with an average value of 5 degs (Figs 5d and e). The angle α_5 is around zero for the first and the last tidal cycles but achieves values of up to 20 degs during the second tidal cycle implying that a significant part of the oscillation occurs in the alongshore direction as well. However these angles are linked to the velocity

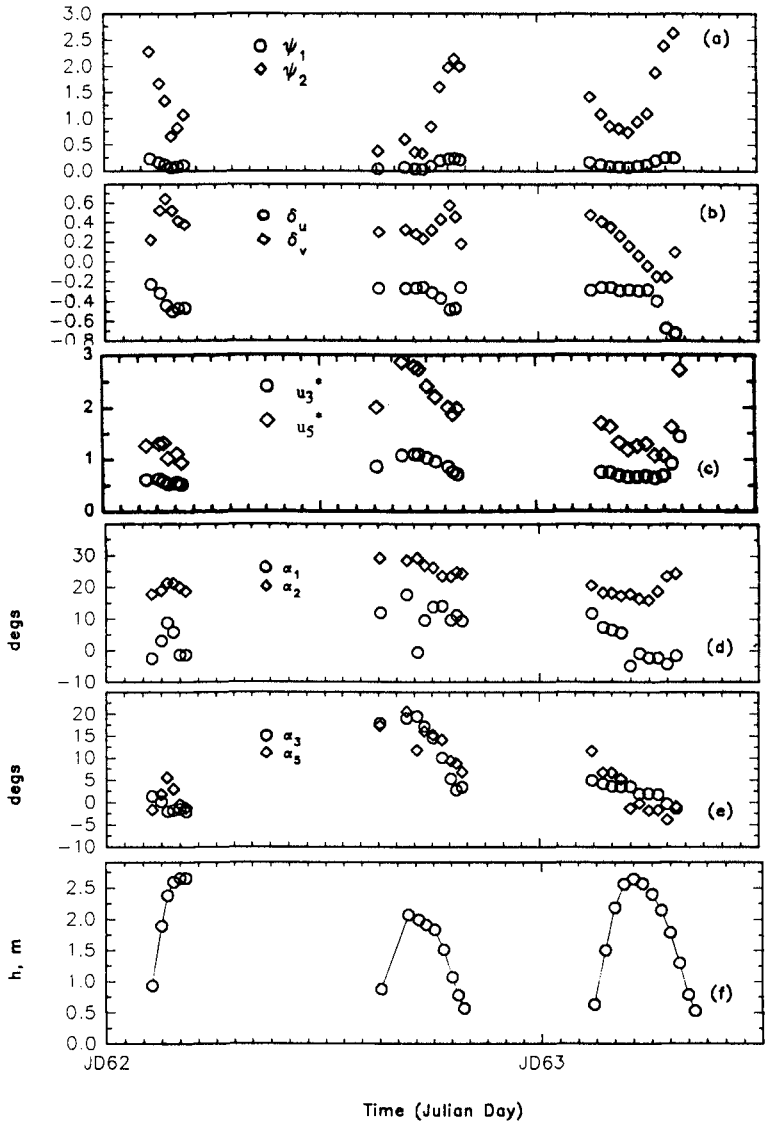

Figure 5. Velocity moment terms used in Bailatd's (1981) energetics sediment transport model (eqs (2) and (3)) as calculated from the measured current velocities from Station D.

moments through their cosine which for the extreme values of 10 and 20degs for the α_1 and α_5 are 0.98 and 0.94 respectively; this implies that omission of these terms will involve an error of 2 and 6%, respectively in the sediment transport rate attributed to these particular terms.

The relative current strength terms δ_u and δ_v vary in accordance with the mean currents observed at the measuring station. It is characteristic that both terms are very important for ridge and runnel beaches reaching absolute values of up to 0.8 which is significantly higher than the average value of 0.01 observed by Guza and Thornton (1985).

The terms $u3^*$ and $u5^*$ express the contributions of the total currents (mean and oscillatory flow) averaged over the whole wave period. In Guza and Thornton's (1985) studies, these were dominated by contributions from the oscillatory component of the cross-shore currents only. In the present study, both oscillatory and mean currents appear to define these moments. It is characteristic that $u3^*$ is almost constant throughout the data collection period, with an average value of 2.5 (standard. deviation 0.34). This value is larger than the theoretical one, derived either assuming a sinusoidal wave ($u3^*=0.42$) or a Gaussian distribution of the wave field ($u3^*=0.56$) with the latter being in good agreement with the field data collected presented by Guza and Thornton (1985). The increased value in the present data set is due to the strong mean flows present which produce an asymmetry of instantaneous flow vector during a wave cycle. The moment $u5^*$ exhibits significant variations throughout the three tidal cycles.

The relative magnitudes of the bedload and suspended load sediment transport and of each individual term of equations (2) and (3) has been examined, assuming that $\epsilon_s=0.025$ and $\epsilon_b=0.20$. Each sediment transport term in eqns (2) and (3) was calculated and then multiplied by the appropriate factor ($\epsilon_b/\tan\phi$, $U_m\epsilon_s/W$). The contribution of each term to the total sediment transport was expressed as a percentage of the total (bedload and suspended load) gross sediment transport rate, with the sign indicating direction of transport. In order to identify any differences in processes under shoaling and breaking waves the analysis was undertaken separately for broken ($H_{rms}/h > 0.20$) and shoaling waves($H_{rms}/h < 0.20$).

Component	Mode	Term	Contribution
Cross-shore	Suspended	$\psi_2\cos\alpha_5$	+55%
		$\delta_u u3^*$	-37%
	Bedload	$\delta_u(0.5+\cos^2\alpha_2)$	+15%
		$\psi_1\cos\alpha_1$	+ 4%
		Others	< 4%
Longshore	Suspended	$\delta_v u3^*$	+70%
		$\psi_2\sin\alpha_5\cos\alpha_5$	+17%
	Bedload	$\delta_v(0.5+\sin^2\alpha_2)$	+16%
		δ_v^3	+ 7%
		Others	< 4

Table 2.Largest terms in energetics sediment transport eqs (2).and (3).

The results suggested that the most important mode of sediment transport is suspended load both in the longshore and cross-shore; this applies to both shoaling and

breaking wave conditions. The most important terms within each mode of transport and for each direction, together with the percentage contribution to the total gross sediment transport rate are shown in Table 2. From these results, it can be seen that suspended load accounts for more than the 80% of the gross sediment transport rate. Thus it can be argued that equations (2) and (3) can be simplified with significant predictive accuracy to:

$$\langle I_x \rangle_s = \frac{\rho \cdot C_f \cdot U_m^4 \cdot \epsilon_s}{W} \cdot (\psi_2 \cos\alpha_S + \delta_u \cdot u3\,') \qquad (8)$$

and

$$\langle I_y \rangle_s = \frac{\rho \cdot C_f \cdot U_m^4 \cdot \epsilon_s}{W} \cdot (\delta_v \cdot u3\,') \qquad (9)$$

for the cross-shore and longshore directions, respectively.

Suspended Sediment Fluxes

Local suspended sediment fluxes from station D and for the lower elevation (9 cm) of SSC measurement are shown in Fig 6 for the cross-shore direction. Mean cross-shore, suspended sediment fluxes dominate; they are directed consistently offshore with maxima occurring at the beginning and the end of the tidal cycle, in shallow water depths where the local resuspension processes are more significant. The absolute values of the mean fluxes are an order of magnitude greater than the oscillatory ones due to gravity and/or infragravity motions. Gravity fluxes are inconsistent; they are directed offshore during the first data cycle, whilst during the second tidal cycle they are contributing to an onshore flux. Finally, during the last tidal cycle they contribute to an onshore

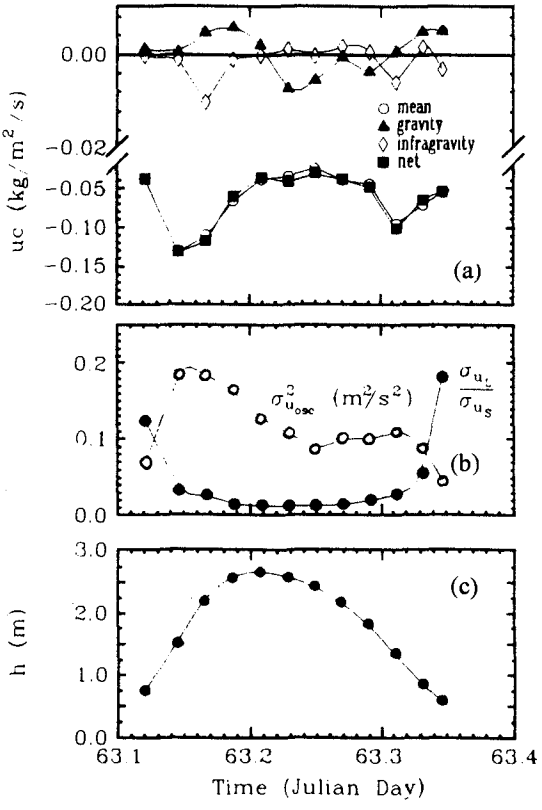

Figure 6. (a) Mean, gravity, infragravity and net local cross-shore suspended sediment flux for the last tidal cycle (Julian day 63) measured at 9 cm above the sea bed. (b) Total variance of oscillatory currents (○) and ratio of infragravity over gravity kinetic energy (•). (c) Local mean water depth (h).

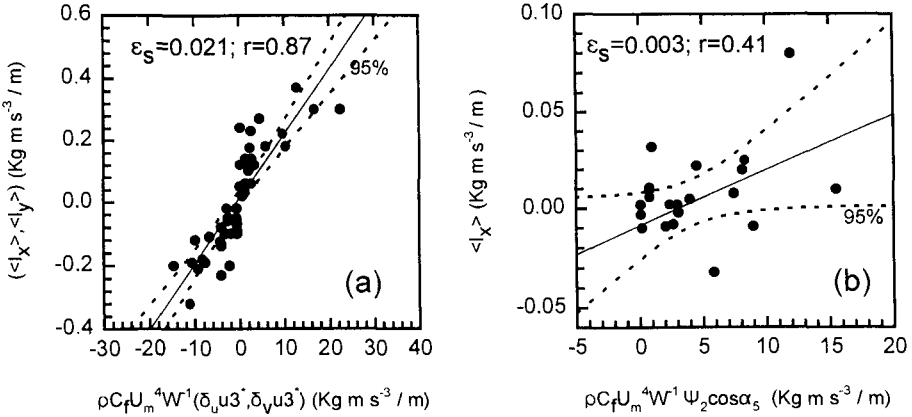

Figure 7. Comparison of measured, depth-integrated immersed weight suspendended sediment transport rats with the terms of eqs (2) and (3). (a) Mean mode of suspended sediment transport (cross-shore, $<I_x>$ and longshore $<I_y>$ data superimposed). (b) Oscillatory mode of transport (cross-shore only).

sediment transport during the flood; during high water the flux is directed offshore and turns again to onshore at the last stage of the ebb tide. The contribution of the infragravity motions is comparable to that of the gravity waves, with the main characteristic being that when the infragravity flux is of any significance it is always directed offshore, in other cases its direction is variable.

Longshore local fluxes (not shown here) are dominated also by the mean fluxes. Both mean and net fluxes are northeasterly (*i.e.* towards the Netherlands). Gravity fluxes although an order of magnitude smaller than the mean, contribute to a northeasterly sediment transport in the direction of wave approach. However, infragravity motions, which result in a southwesterly transport during the first tide, exhibit a variability in direction during the second tidal cycle whilst during the last tidal cycle contribute to a northeasterly transport during the flood and a southwesterly flux during the ebb.

Modelling Suspended Sediment Transport

Depth-integrated values of immersed weight suspended sediment transport rates were obtained by box integrating the measured local suspended sediment fluxes (Voulgaris and Collins, 1996). The lower and upper limits for the integration were the sea bed and 0.5m above the sea bed, respectively. The general patterns observed in the local fluxes analysis were present in the depth-averaged sediment transport rates.

The terms describing sediment transport due to mean currents for both the cross-shore (2nd term in eq. (8)) and longshore directions (eq. (9)) have been combined and

plotted against the predicted mean depth-integrated flux in Figure 6a. A very good agreement was found with a correlation coefficient of 0.87. The efficiency factor (ϵ_s) was determined by regression analysis and was found to be 0.021. The oscillatory component (which is dominated by the gravity mode) of the measured cross-shore suspended sediment transport is plotted against the 2nd term of eq (8) in Figure 7b. There, it can be seen that the correlation is poor; the model always predicts onshore transport due to the waves while the measurements revealed periods of offshore sediment transport. This discrepancy is believed to be due to the presence of vortex ripples which can reverse the sediment transport direction near the bed (Vincent and Green, 1990). Visual observations, during low water, identified ripples with height 0.7cm and wavelength 8.5cm. These were asymmetrical in shape, directed offshore, with curved crests characteristic of ripples occurring under the co-existence of waves and currents. Application of the Wiberg and Harris (1994) model for the period when the intertidal zone was inundated suggested the existence of ripples with height of the order 3 to 5 cm and wavelength 10 to 20cm. The inconsistency between the modelled and visually observed ripple dimensions is attributed to the fact that the latter observations were undertaken during low water when the ripples were washed and flattened out by the swash zone.

Conclusions

In the mid-tidal zone of a macrotidal ridge and runnel beach, under mild conditions, both steady (tidally-induced) and oscillatory currents are equally important for the resuspension of sediment. Their importance is expressed not only in terms of their absolute magnitude but also in terms of wave-current interaction.

Suspended sediment transport is dominated by the mean currents

Bailards (1981) energetics model appears to predict suspended sediment transport due to mean currents quite accurately. However, it fails to predict suspended sediment transport due to wave-induced orbital velocities; this is probably due to the presence of vortex ripples.

The efficiency factor for suspended sediment transport and for the mean mode of transport was found to be 0.021.

Acknowledgments

The authors would like to acknowledge M.P. Wilkin and D.Simmonds for their invaluable assistance. The study was funded by the Commission of the European Community (DG XII) under Contract No. MAS2-CT92-0024-C (C-STAB). This contribution was prepared while G.Voulgaris was at Woods Hole Oceanographic Institution with a Post-Doctoral Award funded by the Mellon Foundation.

References

Aagaard, T. and Greenwood, B.M., 1995. Longshore and Cross-shore Suspended Sediment Transport at Far Infragravity Frequencies in a Barred Environment. Continental Shelf Research, 15(10): 1235-1250.

Bagnold, R.A., 1966. An Approach to the Sediment Transport Problem from General Physics. U.S. Geol. Sur. Prof. Pap. 422-1.

Bailard, A., 1982. Modelling On-Offshore Sediment Transport in the Surfzone. Proc. ASCE 18th Conf. Coastal Eng.: 1419-1438.

Bailard, J.A., 1981. An Energetics Total Load Sediment Transport Model for a Plane Sloping Beach. Journal of Geophysical Research, 86:10,938-10,954.

Bowen, A.J., 1980. Simple Models of Nearshore Sedimentation: Beach Profiles and Alongshore Bars. In: The Coastline of Canada. McCann, S.B. (Editor). Geological Society of Canada, Paper 80-10, Ottawa, pp. 1-11.

De Moor, G., 1991. The Beach Nourishment of Bredene-De Haan and Its Impact on the Beach Morphology and the Coastal Evolution of the Belgian Coast East of Oostende. Proceedings IGU Symposium "Coastal Protection". Nantes, October, 1991.

Guza, R.T. and Thornton E.B., 1985. Velocity Moments in the Nearshore. J. Waterway, Port, Coastal & Ocean Eng., 111(2): 235-256.

King, C.A.M. and Williams, W.E., 1949. The Formation and Movement of Sand Bars by Wave Action. Geographical Journal, 113: 70-85.

Orford, J.D. and Wright, P., 1978. What's In a Name? - Descriptive or Genetic Implications of "Ridge and Runnel" Topography. Marine Geology, 28: M1-M8.

Roelvink, J.A. and Stive, M.J.F., 1989. Bar-Generating Cross-Shore Flow Mechanisms on a Beach. Journal of Geophysical Research, 94(C4): 4785-4800.

Russell,P, Foote, Y. and Huntley, D.A., 1995. An Energetics Approach to Sediment Transport on Macrotidal Beaches. In: Coastal Dynamics '95, ASCE:

Schoonees, J.S. and Theron, A.K., 1995. Evaluation of 10 Cross-Shore Sediment Transport/Morphological Models. Coastal Engineering, 25: 1-41.

Soulsby, R.L., Hamm, L., Lopman, G., Myrhaug, D., Simons, R.R. and Thomas, G.P., 1993. Wave-Current Interaction Within and Outside the Bottom Boundary Layer. Coastal Engineering, 21: 41-69.

Thornton, E.B., Humiston, R.T. and Birkemeier, W., 1996. Bar/Trough Generation on a Natural Beach. Journal of Geophysical Research. 101(C5): 12097-12110.

Vincent, C.E. and Green, M.O., 1990. Field Measurements of the Suspended Sand Concentration Profiles, and of the Resuspension Coefficient γ over Rippled Bed. Journal Geophysical Research, 95: 15591-15601.

Voulgaris, G., 1992. Suspended Sediment Transport in the Nearshore Zone. Department of Oceanography, University of Southampton. Unpublished Ph.D. Thesis, 425pp.

Voulgaris, G. and Collins, M.B, 1996. Suspended Sediment Fluxes: *In:* B.A. O'Connor (Editor). Project MAS2-CT92-0024, Circulation and Sediment Transport Around Banks, CSTAB. Vol 2. Report No CE/05/96. Department of Civil Engineering, University of Liverpool, pp.495-545.

Voulgaris, G. and Simmonds, D., 1996. Incident Waves. *In*: B.A. O'Connor (Editor) Project MAS2-CT92-0024. Circulation and Sediment Transport Around Banks, CSTAB. Vol. 2. Report No CE/05/96. Department of Civil Engineering, University of Liverpool, pp. 451-460..

Wiberg, P.L. and Harris, C.K., 1994. Ripple Geometry in Wave-Dominated Environments. Journal of Geophysical Research, 99(C1): 775-789.